EPJ Web of Conferences **126**, 04042 (2016) DOI: 10.1051/epjconf/201612604042
ICNFP 2015

Perfect Abelian dominance of confinement in mesons and baryons in SU(3) lattice QCD

Naoyuki Sakumichi[1,a] and Hideo Suganuma[2]

[1] *Theoretical Research Division, Nishina Center, RIKEN, Wako, Saitama 351-0198, Japan*
[2] *Department of Physics, Kyoto University, Kitashirakawaoiwake, Sakyo, Kyoto 606-8502, Japan*

Abstract. For a long time, the quark confinement mechanism has been one of the most difficult problems in theoretical physics. In particular, there is no clear correspondence between the confinement and non-Abelian nature of QCD. We study the static interquark potential and its Abelian projection in both mesons and baryons in the maximally Abelian (MA) gauge in SU(3) quenched lattice QCD. Remarkably, we find that the quark confining force in QCD can be perfectly described only with Abelian variables in the MA gauge, which we call "perfect Abelian dominance" of the quark confinement.

1 Introduction

The mechanism of quark confinement is an important long-standing problem in quantum chromodynamics (QCD). To explain the mechanism, Nambu, 't Hooft and Mandelstam [1–3] proposed the dual-superconductor theory in the 1970s. As shown in figure 1, in this theory, the QCD vacuum is assumed to be an electromagnetic dual version of a superconductor, and one-dimensional squeezing of the interquark color-electric flux is caused by the dual version of the Meissner effect, similar to the formation of the Abrikosov vortex in type-II superconductor. The one-dimensional squeezing yields a linear interquark potential at long distance and explain confinement. However, there are two large gaps between the dual superconductor and the QCD vacuum: (i) the dual superconductor is governed by an Abelian U(1) gauge theory, while QCD is a non-Abelian SU(3) gauge theory; (ii) the dual superconductor requires the condensation of color-magnetic monopoles, while QCD does not have such monopoles as elementary degrees of freedom. To fill in the above two gaps, 't Hooft [4, 5] proposed a mathematical procedure of Abelian projection to reduce QCD to an Abelian gauge theory including monopole degrees of freedom. In particular, as a special Abelian projection, the maximally Abelian (MA) projection can extract infrared-relevant Abelian degrees of freedom from QCD in lattice calculations, which is called "Abelian dominance". Figure 2 shows the procedure of the MA projection: (i) the diagonal part of gluons is maximized by minimizing the off-diagonal part under the gauge transformation, which is called MA gauge fixing [6–11]; (ii) SU(3) QCD is projected onto a $U(1)^2$ Abelian gauge theory by dropping the off-diagonal part of gluons. Many lattice QCD studies have shown that the MA-projected Abelian theory well reproduces interquark potential at long distances, i.e, the string tension σ (the infrared linear slope of the potential) is reproduced by the Abelian-projected one σ^{Abel} in both SU(2) [6–10] and SU(3) [12, 13] color QCD.

[a] e-mail: sakumichi.naoyuki@ocha.ac.jp (Present affiliation is Ochanomizu University.)

In this study, we investigate the Abelian dominance of quark confinement of the quark-antiquark ($Q\bar{Q}$) and three-quark (3Q) potentials in SU(3) QCD at the quenched level. Remarkably, we found perfect Abelian dominance of the string tensions in $Q\bar{Q}$ [14] and 3Q [15] systems, i.e., $\sigma^{\mathrm{Abel}} \simeq \sigma$.[1] To obtain $\sigma^{\mathrm{Abel}} \simeq \sigma$, it is necessary to use large-volume lattices of more than about 2 fm [14, 15]. These observations of $\sigma^{\mathrm{Abel}} \simeq \sigma$ indicate that the Abelianization of QCD can be realized without loss of the quark-confining force via the MA projection.

This paper is organized as follows. In Sect. 2, we describe the numerical methods to calculate the MA-projected Abelian theory and the $Q\bar{Q}$ and 3Q potentials. In Sect. 3, we show the numerical results and perfect Abelian dominance of confinement in $Q\bar{Q}$ and 3Q systems. In Sect. 4, we summarize the main results of this study. This paper is based on our previous publications [14, 15], in which the details of the formulations and results are described.

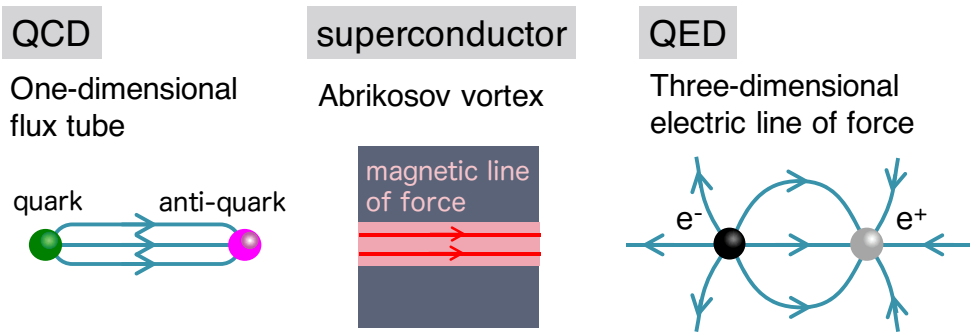

Figure 1. In superconductors, magnetic flux is repelled due to Cooper-pair condensation, and is squeezed into a one-dimensional tube like the Abrikosov vortex. In the dual-superconductor picture, the QCD vacuum is regarded as an electromagnetic dual version of the superconductor: the interquark color-electric flux is squeezed into a one-dimensional form due to magnetic-monopole condensation.

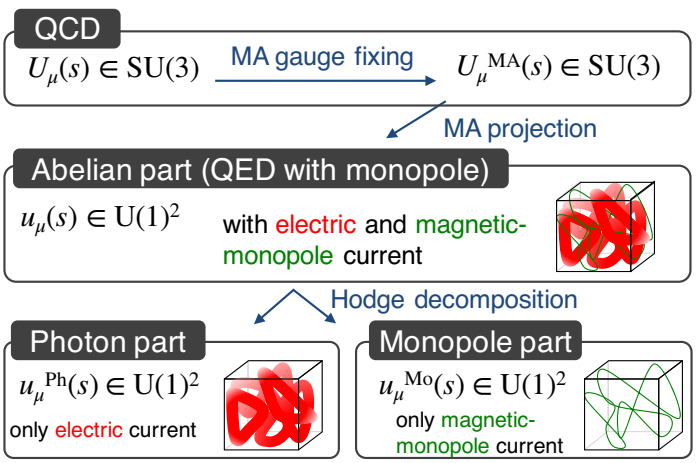

Figure 2. Schematic figure of Abelianization of QCD and the dual-superconductor scenario of confinement. In the MA gauge, QCD becomes Abelian-like, and the monopole current topologically appears. The Abelian part $u_\mu(s)$ is factorized into the regular (photon) part $u_\mu^{\mathrm{Ph}}(s)$ and the singular (monopole) part $u_\mu^{\mathrm{Mo}}(s)$ with respect to the Hodge decomposition as $u_\mu(s) = u_\mu^{\mathrm{Ph}}(s)u_\mu^{\mathrm{Mo}}(s)$. The monopole part has confinement, chiral symmetry breaking, and instantons, while the photon part does not have all of them [9, 17–19].

[1] Perfect Abelian dominance was found also in SU(2) quenched QCD [16]. $\sigma^{\mathrm{Abel}}/\sigma = 1.02(2)$ for $\beta = 2.5$ on 24^4 lattice, when the physical volume is $La \simeq 2.0$ fm.

2 Numerical methods: the MA projection and the QQ and 3Q potentials.

In this study, we perform SU(3) quenched lattice QCD simulations using the standard plaquette action [20]. We investigate $12^3 32$, $16^3 32$, $20^3 32$, and 32^4 lattices at $\beta \equiv 6/g^2 = 5.8$–6.4, with the gauge coupling g. Here, we identify 32 as the temporal sizes and the others (12^3, 16^3, 20^3, 32^3) as the spatial ones. We summarize the simulation condition and related quantities in table 1. We sample the gauge configuration every 500 sweeps, after a thermalization of 20000 sweeps.

The procedure of MA gauge fixing and MA projection in the lattice QCD formalism is shown in figure 2. The link variable

$$U_\mu(s) = \exp(iagA_\mu(s)) \in \mathrm{SU}(3) \tag{1}$$

describes the gauge field, with the lattice spacing a and the gluon field $A_\mu(s)$. To perform the SU(3) MA gauge fixing, we maximize

$$R_{\mathrm{MA}}[U_\mu(s)] \equiv \sum_s \sum_{\mu=1}^{4} \mathrm{tr}\left(U_\mu^\dagger(s)\vec{H}U_\mu(s)\vec{H}\right) = \frac{1}{2}\sum_s \sum_{\mu=1}^{4}\left(\sum_{i=1}^{3}|U_\mu(s)_{ii}|^2 - 1\right) \tag{2}$$

under the SU(3) gauge transformation. Here, $\vec{H} = (T_3, T_8)$ denotes the generators of the Cartan subalgebra. Let $U_\mu^{\mathrm{MA}}(s)$ be the link variables in the MA gauge. The Abelian part of the link variables

$$u_\mu(s) = \exp\left(i\theta_\mu^3(s)T_3 + i\theta_\mu^8(s)T_8\right) \in \mathrm{U}(1)_3 \times \mathrm{U}(1)_8$$

are extracted by maximizing the norm

$$R_{\mathrm{Abel}} \equiv \frac{1}{3}\mathrm{Re}\,\mathrm{tr}\left(U_\mu^{\mathrm{MA}}(s)u_\mu^\dagger(s)\right) \in \left[-\frac{1}{2}, 1\right]. \tag{3}$$

In this study, we numerically maximize R_{MA} in Eq. (2) for each configuration until it converges. Here, we use the overrelaxation method [12] for the maximization algorithm to improve convergence. We remark that there remains the residual $\mathrm{U}(1)^2$ gauge symmetry in the MA gauge. In fact, R_{MA} in Eq. (2) is invariant under the $\mathrm{U}(1)^2$ gauge transformation. Thus, the Abelian link variables $u_\mu(s)$ behave as gauge variables in $\mathrm{U}(1)^2$ lattice gauge theory, which is similar to the compact QED. As mentioned above, the MA-projected Abelian theory has not only the electric current, but also the magnetic-monopole current.

Table 1. The simulation conditions (β, the lattice size L^3L_t, and the gauge configuration number N_{con}), the related quantities (lattice spacing a and the physical spatial size La), and the results of the string tension ratio $\sigma^{\mathrm{Abel}}/\sigma$, $\sigma_{3\mathrm{Q}}^{\mathrm{Abel}}/\sigma_{3\mathrm{Q}}$. The lattice spacing a is determined so as to reproduce the string tension of $\sigma = 0.89$ GeV/fm in the $\mathrm{Q\bar{Q}}$ potential. The label of (ET) means the fit analysis only with the lattice data of equilateral-triangle 3Q configurations. The values in parentheses denote the standard error.

β	L^3L_t	N_{con}	a [fm]	La [fm]	$\sigma^{\mathrm{Abel}}/\sigma$	$\sigma_{3\mathrm{Q}}^{\mathrm{Abel}}/\sigma_{3\mathrm{Q}}$	$\sigma_{3\mathrm{Q}}^{\mathrm{Abel}}/\sigma_{3\mathrm{Q}}$(ET)
6.4	32^4	200	0.0582(2)	1.86(1)	1.015(09)		
6.0	32^4	200	0.1022(5)	3.27(1)	1.009(10)		
5.8	$16^3 32$	2000	0.148(1)	2.37(3)	0.99(3)	0.97(1)	1.01(3)
6.0	$20^3 32$	1000	0.1022(5)	2.05(1)	0.97(1)	0.95(1)	0.97(3)
6.0	$16^3 32$	600	0.102(1)	1.64(1)	0.94(1)		
6.0	$12^3 32$	400	0.104(1)	1.25(4)	0.94(3)		
6.2	$16^3 32$	400	0.075(1)	1.20(1)	0.95(2)		

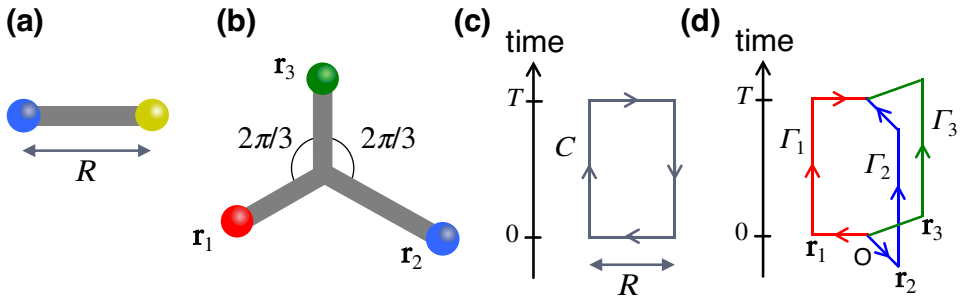

Figure 3. (a) The flux-tube configuration of the mesonic $Q\bar{Q}$ system. (b) The flux-tube configuration of the baryonic 3Q system with the minimal value of the total flux-tube length. There appears a physical junction linking the three flux tubes at the Fermat point. (c) The trajectory of the ($Q\bar{Q}$) Wilson loop W. The quark and anti-quark are generated at $t = 0$, are spatially fixed in $\mathbb{R}^3$ for $0 < t < T$, and are annihilated at $t = T$. (d) The trajectory of the 3Q Wilson loop W_{3Q}. The three quarks are generated at $t = 0$, are spatially fixed in $\mathbb{R}^3$ for $0 < t < T$, and are annihilated at $t = T$.

As shown in figure 3, we calculate the $Q\bar{Q}$ and 3Q potentials [21, 22]

$$V(r) = -\lim_{t\to\infty} \frac{1}{t} \ln \left\langle W\left[U_\mu(s)\right]\right\rangle, \tag{4}$$

$$V_{3Q}(r) = -\lim_{t\to\infty} \frac{1}{t} \ln \left\langle W_{3Q}\left[U_\mu(s)\right]\right\rangle \tag{5}$$

from the $Q\bar{Q}$ Wilson loop $W\left[U_\mu(s)\right] \equiv \mathrm{tr}\left(\prod_C U_\mu(s)\right)$ and the 3Q Wilson loop

$$W_{3Q}\left[U_\mu(s)\right] \equiv \frac{1}{3!} \sum_{a,b,c} \sum_{a'b'c'} \epsilon_{abc}\epsilon_{a'b'c'} X_1^{aa'} X_2^{bb'} X_3^{cc'}, \tag{6}$$

respectively. Here, $\langle \cdots \rangle$ is the statistical average over the gauge configurations. In the $Q\bar{Q}$ and 3Q Wilson loops, $\prod_C U_\mu(s)$ and $X_k \equiv \prod_{\Gamma_k} U_\mu(s)$ are the path-ordered product of the link variables along the path denoted by C and Γ_k in figure 3-(c) and (d), respectively. The $Q\bar{Q}$ and 3Q Wilson loops represent that the gauge-invariant $Q\bar{Q}$ or 3Q state is generated at $t = 0$ and is annihilated at $t = T$ with the quarks spatially fixed in $\mathbb{R}^3$ for $0 < t < T$.

We also calculate the MA projection of the $Q\bar{Q}$ and 3Q potentials

$$V^{\mathrm{Abel}}(r) = -\lim_{t\to\infty} \frac{1}{t} \ln \left\langle W\left[u_\mu(s)\right]\right\rangle, \tag{7}$$

$$V_{3Q}^{\mathrm{Abel}}(r) = -\lim_{t\to\infty} \frac{1}{t} \ln \left\langle W_{3Q}\left[u_\mu(s)\right]\right\rangle \tag{8}$$

from the Abelian Wilson loop in the MA gauge $W\left[u_\mu(s)\right]$ and the 3Q one $W_{3Q}\left[u_\mu(s)\right]$, respectively. They are invariant under the residual Abelian gauge transformation.

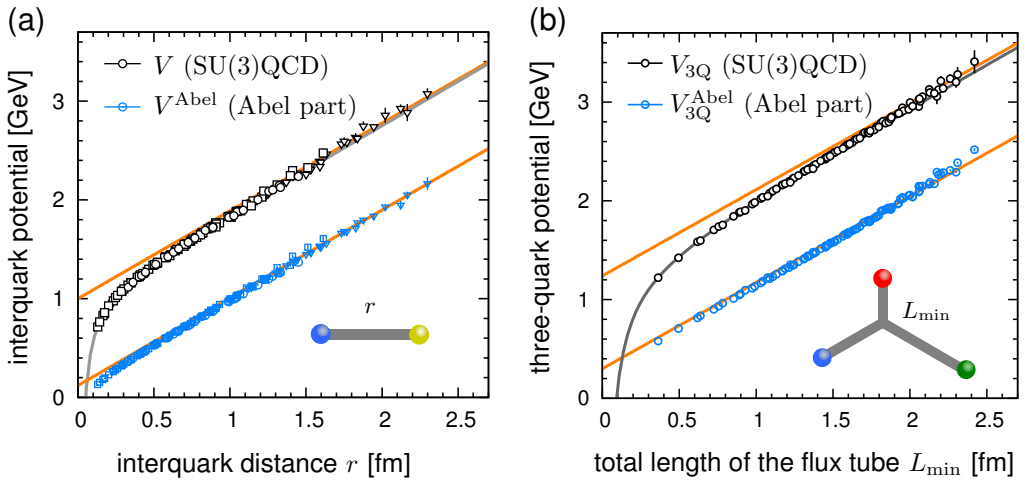

Figure 4. SU(3) quenched lattice QCD results of MA projection of (a) $Q\bar{Q}$ and (b) 3Q potentials taken from Refs. [14] and [15], respectively. In each panel, the black and blue labels denote the original SU(3) potential and the Abelian part, respectively. The circles, triangles, and squares denote the results from $16^3 32$ lattice at $\beta = 5.8$, 32^4 lattices at 6.0 and 6.4, respectively. The gray curves are obtained by the best fit with Eqs. (9) and (11) (Y ansatz). The slopes of the *parallel* orange lines for the panels (a) and (b) are σ and σ_{3Q}, respectively. The error bars in each panel denote the statistical errors estimated with the jackknife method.

3 Perfect Abelian dominance of confinement in mesons and baryons

In this section, we explain lattice QCD results of the original $Q\bar{Q}$ and 3Q potentials $V(r)$ and V_{3Q}, and their Abelian part, $V_{\rm Abel}(r)$ and $V_{3Q}^{\rm Abel}$. Figure 4 (a) shows the $Q\bar{Q}$ potential on the 32^4 lattice at $\beta = 6.4, 6.0$ and on the $16^3 32$ lattice at $\beta = 5.8$. Here, we investigate the on- and off-axis interquark directions as $(1,0,0), (1,1,0), (1,1,1), (2,1,0), (2,1,1), (2,2,1)$. Figure 4 (b) shows the 3Q potential on the $16^3 32$ lattice at $\beta = 5.8$.

First, we explain that the original $Q\bar{Q}$ and 3Q potentials are well reproduced by

$$V(r) = \sigma r - \frac{A}{r} + C, \tag{9}$$

$$V_{3Q}(\mathbf{r}_1, \mathbf{r}_2, \mathbf{r}_3) = \sigma_{3Q} L_{\rm min} - \sum_{i<j} \frac{A_{3Q}}{|\mathbf{r}_i - \mathbf{r}_j|} + C_{3Q}, \tag{10}$$

respectively. The form (10) is called the Y ansatz [21, 22]. Here, $\mathbf{r}_1, \mathbf{r}_2$, and $\mathbf{r}_3$ are the positions of the three quarks, and $L_{\rm min}$ is the minimum flux-tube length connecting the three quarks as shown in figure 3 (b). In fact, figure 4 (a) shows that the best-fit of Eq. (9) (gray curve) well reproduces the original $Q\bar{Q}$ potential. The 3Q potential is rather complicated, because it generally depends on the relative position of the three quarks. However, as shown in figure 4 (b), we can see that all the lattice data of V_{3Q} (at $\beta = 5.8$) are approximately described by a single-valued function of the total length of the flux tube, $L_{\rm min}$. The main reason is that the three-body confinement term $\sigma_{3Q} L_{\rm min}$ is relevant in the Y ansatz (10) except for short distances. When the 3Q system forms an equilateral triangle, one

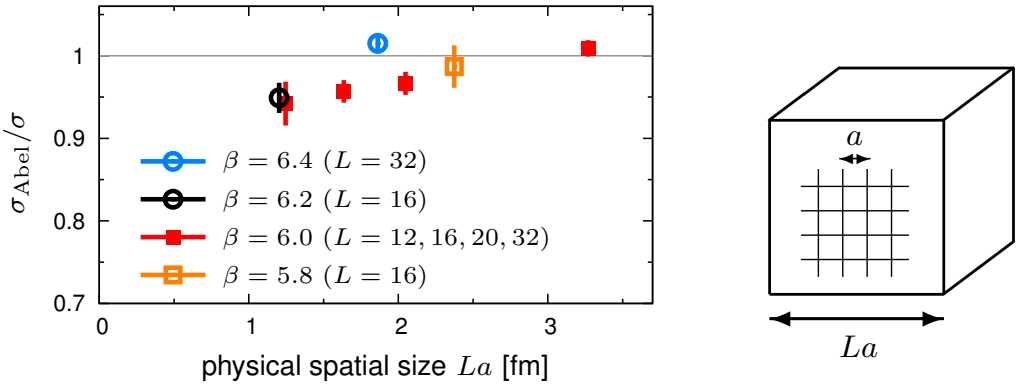

Figure 5. Physical spatial-size dependence of $\sigma_{\rm Abel}/\sigma$ taken from Ref. [15]. Here, σ and $\sigma_{\rm Abel}$ are the string tensions of the Q$\bar{\rm Q}$ potential for SU(3) QCD and the Abelian part, respectively. Perfect Abelian dominance ($\sigma_{\rm Abel}/\sigma \simeq 1$) seems to be realized when the spatial size La is larger than about 2 fm.

finds $L_{\rm min} = \sqrt{3}\left|\mathbf{r}_i - \mathbf{r}_j\right|$ for any $i \neq j$, and the Y ansatz (10) becomes

$$V_{\rm 3Q}(L_{\rm min}) = \sigma_{\rm 3Q} L_{\rm min} - 3\sqrt{3}\,\frac{A_{\rm 3Q}}{L_{\rm min}} + C_{\rm 3Q}. \tag{11}$$

In figure 4 (b), we show that the best-fit of Eq. (11) (gray curve) well reproduces all the lattice data of original 3Q potential, other than the equilateral-triangle 3Q systems. These functional forms (9) and (10) indicate the flux-tube picture on the confinement mechanism as shown in figure 3 (a) and (b); that is, valence quarks are linked by the color flux tube as a quasi-one-dimensional object [20, 23]. The strength of quark confinement is controlled by the string tension of the flux tube, σ or $\sigma_{\rm 3Q}$, i.e., the infrared linear slopes of the confinement terms in both potentials.

Second, we explain "perfect Abelian dominance" of confinement in mesonic Q$\bar{\rm Q}$ potential [14]. In figure 4 (a), the Coulomb-plus-linear ansatz (9) well reproduce all the lattice data $V(r)$. For a larger interquark distance r than 1 fm, the linear quark-confining potential $\sigma r + C$ describes $V(r)$ [upper straight line in figure 4 (a)]. The Abelian part $V^{\rm Abel}(r)$ (blue labels) has a significant agreement with $\sigma r + C'$ [lower straight line in figure 4 (a)] at large distances, which illuminates "perfect Abelian dominance" of confinement in the Q$\bar{\rm Q}$ potential. It is likely that a large physical volume approximately larger than $(2\ {\rm fm})^3$ is necessary for the perfect Abelian dominance of the string tension, as shown in table 1 and figure 5.

Third, we explain "perfect Abelian dominance" of confinement in baryonic 3Q potential [15]. We note that the perfect Abelian dominance of the Q$\bar{\rm Q}$ potential does not necessarily mean that of the 3Q potential, because one cannot superpose solutions in QCD even at the classical level. Indeed, a 3Q system cannot be described by the superposition of the interaction between two quarks, as is suggested from the functional form (10) of the 3Q potential [21, 22]. We find, however, "perfect Abelian dominance" of confinement in baryonic 3Q potential with an accuracy within a few percent deviation as described below. In figure 4 (b), the Y ansatz (11) well reproduces all the lattice data $V_{\rm 3Q}(r)$. When the total flux-tube length $L_{\rm min}$ is larger than 1 fm, $V_{\rm 3Q}$ is described by the linear 3Q-confining potential $\sigma_{\rm 3Q} L_{\rm min} + C_{\rm 3Q}$ [upper straight line in figure 4 (b)]. Remarkably, the Abelian part $V^{\rm Abel}(r)$ has a significant agreement with $\sigma_{\rm 3Q} L_{\rm min} + C'_{\rm 3Q}$ [lower straight line in figure 4 (b)] at large distances, other than the equilateral-triangle 3Q systems, which is the plausible evidence for perfect

Abelian dominance of quark confinement in baryons. The ratios of the string tensions, $\sigma_{3Q}^{\rm Abel}/\sigma_{3Q}$ are summarized in table 1.

4 Summary

We have studied the MA projection of quark confinement in the mesonic quark-antiquark and baryonic three-quark potentials in the SU(3) QCD with several spacings and volume lattices. We have found perfect Abelian dominance of the string tension with an accuracy within a few percent deviation, $\sigma \simeq \sigma^{\rm Abel} \simeq \sigma_{3Q} \simeq \sigma_{3Q}^{\rm Abel}$, in $Q\bar{Q}$ and 3Q potentials simultaneously. In spite of the non-Abelian nature of QCD, quark confinement is entirely kept in the Abelian sector of QCD in the MA gauge. In other words, Abelianization of QCD can be realized without the loss of the quark-confining force via the MA projection. Such Abelianization scheme of QCD is expected to partially reduce the difficulty stemming from non-Abelian nature of QCD, and is meaningful to understand the quark confinement mechanism.

Acknowledgments

The authors thank Hideaki Iida and Toru T. Takahashi. N. S. is supported by a Grant-in-Aid for JSPS Fellows and by JSPS KAKENHI Grant 250588, 15K17725. H. S. is supported by the Grant for Scientific Research [No.15K05076] from the Ministry of Education, Science and Technology of Japan. The lattice calculations were partially performed on NEC-SX8R at Osaka University. This work was partially supported by RIKEN iTHES Project.

References

[1] Y. Nambu, Phys. Rev. D **10**, 4262 (1974).
[2] G. 't Hooft, in *High Energy Physics*, (Editorice Compositori, Bologna, 1975).
[3] S. Mandelstam, Phys. Rep. **23**, 245 (1976).
[4] G. 't Hooft, Nucl. Phys. **B190**, 455 (1981).
[5] Z. F. Ezawa and A. Iwazaki, Phys. Rev. D **25**, 2681 (1982).
[6] A. S. Kronfeld, G. Schierholz, and U.-J. Wiese, Nucl. Phys. **B293** 461 (1987).
[7] A. S. Kronfeld, M. L. Laursen, G. Schierholz, and U.-J. Wiese, Phys. Lett. B **198**, 516 (1987).
[8] T. Suzuki and I. Yotsuyanagi, Phys. Rev. D **42**, 4257 (1990).
[9] J. D. Stack, S. D. Neiman, and R. J. Wensley, Phys. Rev. D **50**, 3399 (1994).
[10] K. Amemiya and H. Suganuma, Phys. Rev. D **60**, 114509 (1999).
[11] M. A. L. Capri, D. Fiorentini, and S. P. Sorella, Phys. Rev. D **91**, 125004 (2015).
[12] J. D. Stack, W. W. Tucker, and R. J. Wensley, Nucl. Phys. **B639**, 203 (2002).
[13] V. G. Bornyakov *et al.* (DIK Collaboration), Phys. Rev. D **70**, 074511 (2004); **70**, 054506 (2004).
[14] N. Sakumichi and H. Suganuma, Phys. Rev. D **90**, 111501 (2014).
[15] N. Sakumichi and H. Suganuma, Phys. Rev. D **92**, 034511 (2015).
[16] S. Kato, K.-I. Kondo, and A. Shibata, Phys. Rev. D **91**, 034506 (2015).
[17] O. Miyamura, Phys. Lett. B **353**, 91 (1995).
[18] R. M. Woloshyn, Phys. Rev. D **51**, 6411 (1995).
[19] H. Suganuma, A. Tanaka, S. Sasaki, and O. Miyamura, Nucl. Phys. **B** (Proc. Suppl.) **47**, 302 (1996).

[20] H. J. Rothe, *Lattice Gauge Theories*, 4th ed. (World Scientific, Singapore, 2012), and references therein.
[21] T. T. Takahashi, H. Matsufuru, Y. Nemoto, and H. Suganuma, Phys. Rev. Lett. **86**, 18 (2001).
[22] T. T. Takahashi, H. Suganuma, Y. Nemoto, and H. Matsufuru, Phys. Rev. D **65**, 114509 (2002).
[23] H. Ichie, V. Bornyakov, T. Streuer, and G. Schierholz, Nucl. Phys. **A721**, C899 (2003).